Electronic Supplement to

FD3D_TSN: A fast and simple code for dynamic rupture simulations with GPU acceleration

by J. Premus, F. Gallovic, L. Hanyk, and A.-A. Gabriel

Here, we describe the implementation of the fault boundary condition in the finite difference (FD) code FD3D_TSN. Dynamic rupture models treat the source of seismic wave propagation as shear rupture under compression across a frictional interface between elastic half-spaces. We consider two types of widely used friction laws - linear slip-weakening and rate-and-state fast-velocity-weakening. When using a staggered grid approach, the components of velocity and stress are not calculated at the same node. Instead, some components are calculated away from the fault plane only, requiring special treatment of the boundary. We use a traction-at-split-node implementation of the dynamic rupture fault boundary conditions as developed by Dalguer and Day (2007)

1 Dynamic rupture fault boundary condition

The fault plane divides the modeling domain into two half-spaces, denoted as $'+'$ and $'-'$ as in Fig. 1. We define slip s_i as a discontinuity in the displacement vector u_i across the fault,

$$s_i(\mathbf{x},t) = u_i^+(\mathbf{x},t) - u_i^-(\mathbf{x},t), \tag{1}$$

and slip rate as a discontinuity in velocity v_i,

$$\dot{s}_i(\mathbf{x},t) = v_i^+(\mathbf{x},t) - v_i^-(\mathbf{x},t), \tag{2}$$

with absolute values denoted as s and $\dot{s}$, respectively.

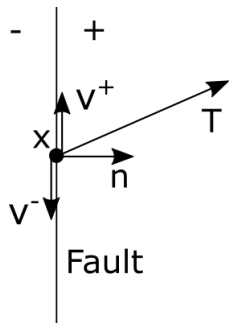

Figure 1: Schematic of the fault variables at point $\mathbf{x}$ – normal to the fault n_i, discontinuous velocity $v_i^+$and v_i^-, and continuous traction T_i.

Let n_i be a unit normal vector to the fault that points into the '+' half-space, and $T_i(\mathbf{x},\mathbf{n},t) = \sigma_{ij}n_j$ is the traction on the fault. Since shear faulting is assumed, continuity of the normal components of displacement u_i^n and velocity v_i^n is required,

$$0 = u_i^{n+}(\mathbf{x},t) - u_i^{n-}(\mathbf{x},t), \tag{3}$$

$$0 = v_i^{n+}(\mathbf{x}, t) - v_i^{n-}(\mathbf{x}, t). \tag{4}$$

Traction $T_i(\mathbf{x}, \mathbf{n}, t)$ is continuous across the fault.

Let $S(\mathbf{x}, t)$ be the frictional strength. The value of shear traction $T^s(\mathbf{x}, \mathbf{n}, t)$ at the fault is bounded by the frictional strength,

$$T^s(\mathbf{x}, t) \leq S(\mathbf{x}, t). \tag{5}$$

Additionally, we define trial shear traction T_i^T, calculated as traction if no slip occurs (i. e., frictional strength S was higher then T^T).

Slip rate and traction are set to be colinear,

$$T_i^s(\mathbf{x}, t)\dot{s}(\mathbf{x}, t) - S(\mathbf{x}, t)\dot{s}_i(\mathbf{x}, t) = 0. \tag{6}$$

The magnitude of traction in the case of slip is relaxed to equal the frictional strength $S(\mathbf{x}, t)$.

The introduction of a non-planar (or even just a dipping yet planar) fault geometry into this regular grid formulation is complicated. Cruz-Atienza et al. (2007) introduced a stable non-planar model for the case of the partially staggered grid. Curvilinear transformation approaches (Duru and Dunham, 2016; Duru et al., 2018, e.g.) are out of the scope of the presented manuscript.

Here, only a vertical planar fault is assumed. All derivations fix the fault plane in the $1-3$ plane. The following symmetries and anti-symmetries of stress and velocity components hold along a fault in the $1-3$ plane (assuming the same material parameters on both sides of the fault plane):

$$v_1^+ = -v_1^- \qquad v_2^+ = +v_2^- \qquad v_3^+ = -v_3^- \tag{7}$$
$$\sigma_{11}^+ = -\sigma_{11}^- \qquad \sigma_{22}^+ = \sigma_{22}^- \qquad \sigma_{33}^+ = -\sigma_{33}^- \tag{8}$$
$$\sigma_{12}^+ = +\sigma_{12}^- \qquad \sigma_{13}^+ = -\sigma_{13}^- \qquad \sigma_{23}^+ = +\sigma_{23}^- \tag{9}$$

2 Traction-at-split-node implementation

Firstly, the traction-at-split-node implementation of the dynamic rupture fault boundary condition is introduced independently of a chosen FD grid – all components of velocity and stress are expected to be all in a single node. The concrete application, using a specific staggered grid scheme, is then described in the second half of the section.

Every node on the fault plane belongs to both half-spaces $'+'$ and $'-'$. To obtain a complete separation into two half-spaces, each of these nodes is split into two split nodes. Velocity and stress components are defined separately for both split nodes and denoted by $'+'$ and $'-'$ signs. The mass of the split node is calculated as $M^{\pm} = \Delta h^3 \rho^{\pm}/2$ – the fault is cutting its FD 'cube' with side length Δh) in half. Traction T_i is shared for both split nodes.

In both halfspaces, the elastodynamic force acts upon the split nodes and is equal to the right hand side of the elastodynamics equation:

$$f_i^{\pm} = \sigma_{ij,j}. \tag{10}$$

Equation (10) represents the body force of the half-space, without the surface (fault) force – for the calculation of this force, the fault is considered to be a free surface.

Split nodes are coupled through traction T_i that generates a surface force f_i^c. This force is of the same magnitude for both split nodes, but of opposite orientation. For the $'-'$ side it yields

$$f_i^c = \Delta h^2 (T_i - T_i^0), \tag{11}$$

where T_i^0 is a traction at the initial state of equilibrium.

The acceleration at split nodes can be derived from Newton's 2nd law:

$$\frac{\partial v_i^{\pm}}{\partial t} = (f_i^{\pm} \mp f_i^c)/M^{\pm}. \tag{12}$$

It is introduced into the FD equations as the right hand side of the updating scheme for the velocity components at the fault plane,

$$(v_i^{\pm})^{N^1} = (v_i^{\pm})^N + \Delta t \left[(f_i^{\pm})^{N^{\frac{1}{2}}} \mp \Delta h^2 \left((T_i)^{N^{\frac{1}{2}}} - T_i^0 \right) \right] / M^{\pm}. \tag{13}$$

The slip rate is calculated from (2), as a difference between the velocity values in both split nodes using (13),

$$(\dot{s}_i)^{N^1} = (\dot{s}_i)^N + \Delta t \left[\frac{(f_i^+)^{N^{\frac{1}{2}}}}{M^+} - \frac{(f_i^-)^{N^{\frac{1}{2}}}}{M^-} + \frac{(T_i)^{N^{\frac{1}{2}}} - T_i^0}{\Delta h^{-2} M^-} - \frac{(T_i)^{N^{\frac{1}{2}}} - T_i^0}{\Delta h^{-2} M^+} \right], \tag{14}$$

which can be rearranged to

$$(\dot{s}_i)^{N^1} = (\dot{s}_i)^N + \frac{\Delta t \, (M^- + M^+)}{\Delta h^{-2} M^- M^+} \left[\frac{M^- (f_i^+)^{N^{\frac{1}{2}}} - M^+ (f_i^-)^{N^{\frac{1}{2}}}}{\Delta h^2 (M^- + M^+)} + (T_i)^{N^{\frac{1}{2}}} - T_i^0 \right]. \tag{15}$$

Next we distinguish between two cases: exhibiting zero or non-zero slip rate $(\dot{s}_i)^{N^1}$. The traction in the former case is equal to trial traction T_i^T. We can simply express it from equation (15) considering $(\dot{s}_i)^{N^1} = 0$:

$$(T_i^T)^{N^{\frac{1}{2}}} = T_i^0 + \frac{\Delta t^{-1} M^- M^+ (\dot{s}_i)^N + M^- (f_i^+)^{N^{\frac{1}{2}}} - M^+ (f_i^-)^{N^{\frac{1}{2}}}}{\Delta h^2 (M^- + M^+)}, \tag{16}$$

while traction in the slipping case is smaller then thus calculated trial traction, and its absolute value is equal to the friction S.

This result is valid for a general fault geometry. In the following, we assume vertical planar fault in the $1-3$ plane. This means that the trial traction has a normal component of $(T_2^T)^{N^{\frac{1}{2}}}$ and two shear components $(T_1^T)^{N^{\frac{1}{2}}}$ and $(T_3^T)^{N^{\frac{1}{2}}}$.

When the value of trial shear traction $(T^T)^{N^{\frac{1}{2}}}$ is higher than frictional force $S^{N^{\frac{1}{2}}}$, slip occurs and $(\dot{s})^{n^1} \neq 0$. Conditions (3) and (4) need to be enforced. In the case when the fault is slipping, we acquire difference between the trial traction and the traction by subtracting (15) in the first case $(\dot{s}^{N^1} = 0, (T_i)^{N^{\frac{1}{2}}} = (T_i^T)^{N^{\frac{1}{2}}})$ from the same equation in the second case $(\dot{s}^{N^1} \neq 0)$, which leads to

$$(\dot{s}_i)^{N^1} = \Delta t \frac{\Delta h^2 (M^- + M^+)}{M^- M^+} \left((T_i)^{N^{\frac{1}{2}}} - (T_i^T)^{N^{\frac{1}{2}}} \right). \tag{17}$$

Time staggered position of velocity and stress implies, that the traction is calculated at time $(N+\frac{1}{2})\Delta t$, while the slip rate at the time $(N+1)\Delta t$. However, these quantities are both needed in the collinearity condition (6). Evaluation of both quantities at a given time step requires interpolation, which can cause unwanted oscillations. Instead, we use values at different time steps,

$$(T_i)^{N\frac{1}{2}}\dot{s}^{N1} - S^{N\frac{1}{2}}(\dot{s}_i)^{N1} = 0, \tag{18}$$

and inserting (17) in (18) yields:

$$\left(S^{N\frac{1}{2}} + (\Delta T)^{N\frac{1}{2}}\right)(T_i)^{N\frac{1}{2}} = S^{N\frac{1}{2}}(T_i^T)^{N\frac{1}{2}}. \tag{19}$$

Here $(\Delta T)^{N\frac{1}{2}}$ is the absolute value of the difference between the shear traction and the shear trial traction. This equation ties the value of $(T_i)^{N\frac{1}{2}}$ with frictional force $S^{N\frac{1}{2}}$. Solution to equation (19),

$$(T_i)^{N\frac{1}{2}} = S^{N\frac{1}{2}}\frac{(T_i^T)^{N\frac{1}{2}}}{(T^T)^{N\frac{1}{2}}}, \tag{20}$$

also fulfills the condition (3).

The final equation for shear traction is:

$$(T_i)^{N\frac{1}{2}} = \begin{cases} (T_i^T)^{N\frac{1}{2}}, & \text{if } (T^T)^{N\frac{1}{2}} \leq S^{N\frac{1}{2}} \\ S^{N\frac{1}{2}}\frac{(T_i^T)^{N\frac{1}{2}}}{(T^T)^{N\frac{1}{2}}}, & \text{if } (T^T)^{N\frac{1}{2}} > S^{N\frac{1}{2}}, \end{cases} \qquad i = 1, 3. \tag{21}$$

In this case, the normal value of traction does not change.

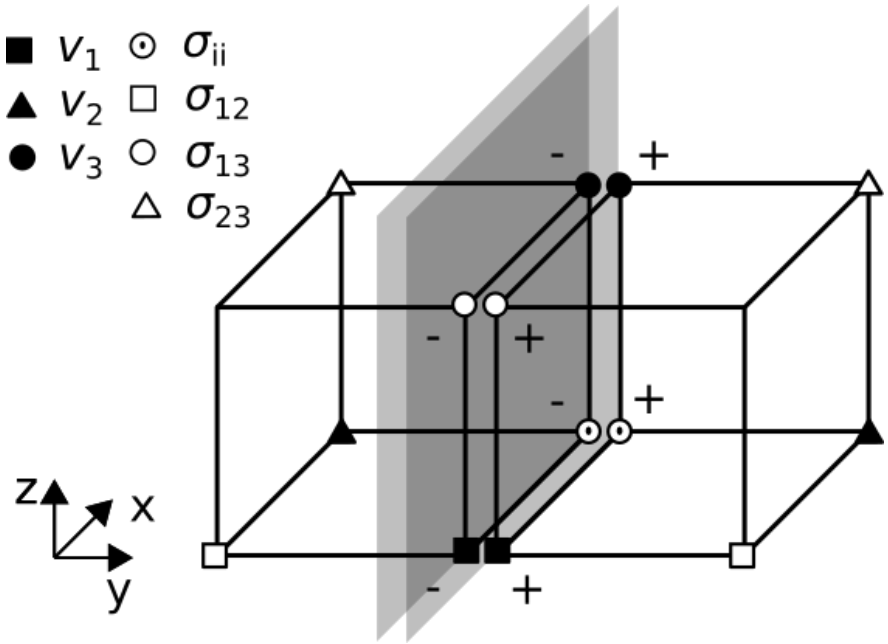

Figure 2: Fault plane dividing the FD staggered grid, when a traction-at-split-nodes approach is applied. Discontinuous components of both velocity and stress at the fault plane are denoted $'+'$ and $'-'$.

Implementation of the traction-at-split-node method into the staggered grid is described next, following (Dalguer and Day, 2007). All components directly at the fault need to be calculated using modified FD equations, which take into account the division of the space by the fault boundary. The exception is σ_{13}, which does not require knowledge of any velocity components at nodes on the other side of the fault. Discontinuous $\sigma_{13}^{\pm}$ can be therefore acquired on both sides using the second or fourth order FD operators.

Shear velocity components $(v_1^{\pm})_{I,J_F,K}$ and $(v_3^{\pm})_{I^{\frac{1}{2}},J_F,K^{\frac{1}{2}}}$ are calculated from (13). Index J_F denotes components directly at the fault. Elastodynamic forces at the fault $(f_1^{\pm})_{I,K}$ and $(f_3^{\pm})_{I^{\frac{1}{2}},K^{\frac{1}{2}}}$ need to be calculated using second order FD along the 1 and 3 axes, but just one-sided FD along the 2 axis. For the purpose of the volume force calculation (10), the traction components σ_{12} and σ_{23} are considered zero at the boundary, leading to:

$$(f_1^{\pm})_{I,K} = \Delta h^2 \Big[(D_1^{(2)} \sigma_{11}^{\pm})_{I,J_F,K} + (D_3^{(2)} \sigma_{13}^{\pm})_{I,J_F,K} \pm (\sigma_{12})_{I,J_F^{\pm\frac{1}{2}},K} \Big] \tag{22}$$

$$(f_3^{\pm})_{I^{\frac{1}{2}},K^{\frac{1}{2}}} = \Delta h^2 \Big[(D_1^{(2)} \sigma_{13}^{\pm})_{I^{\frac{1}{2}},J_F,K^{\frac{1}{2}}} + (D_3^{(2)} \sigma_{33}^{\pm})_{I^{\frac{1}{2}},J_F,K^{\frac{1}{2}}} \pm (\sigma_{23})_{I^{\frac{1}{2}},J_F^{\pm\frac{1}{2}},K^{\frac{1}{2}}} \Big], \tag{23}$$

where $D_i^{(k)}$ means finite difference operator of the k-th order in direction i.

We acquire the final equations for the trial traction and slip rate by:

- inserting these forces into (15) and (13),
- applying (7),
- and assuming $M^+ = M^- = 1/2\Delta h^2 \rho$,

leading to:

$$\begin{aligned}
(T_1^T)^{N^{\frac{1}{2}}} &= T_1^0 - \frac{1}{2}\frac{\Delta h}{\Delta t}\rho v_1^N - (R_1^-)^{N^{\frac{1}{2}}}, \\
(T_3^T)^{N^{\frac{1}{2}}} &= T_3^0 - \frac{1}{2}\frac{\Delta h}{\Delta t}\rho v_3^N - (R_3^-)^{N^{\frac{1}{2}}}, \\
(v_1^-)^{N^1} &= (v_1^-)^N + \frac{2\Delta t}{\Delta h \rho}\left[(R_1^-)^{N^{\frac{1}{2}}} + (T_1)^{N^{\frac{1}{2}}} - T_1^0 \right], \\
(v_3^-)^{N^1} &= (v_3^-)^N + \frac{2\Delta t}{\Delta h \rho}\left[(R_3^-)^{N^{\frac{1}{2}}} + (T_3)^{N^{\frac{1}{2}}} - T_3^0 \right],
\end{aligned} \tag{24}$$

with

$$\begin{aligned}
(R_1^-)^{N^{\frac{1}{2}}} &= \frac{1}{4}\Big[(D_1^{(2)} \sigma_{11}^-) + (D_3^{(2)} \sigma_{13}^-) \Big] - (\sigma_{12})_{I,J_F^{-\frac{1}{2}},K}, \\
(R_3^-)^{N^{\frac{1}{2}}} &= \frac{1}{4}\Big[(D_1^{(2)} \sigma_{13}^-) + (D_3^{(2)} \sigma_{33}^-) \Big] - (\sigma_{23})_{I^{\frac{1}{2}},J_F^{-\frac{1}{2}},K^{\frac{1}{2}}}.
\end{aligned} \tag{25}$$

Note that the $'1'$ components are calculated at nodes (I, J_F, K), while the $'3'$ components at $(I^{\frac{1}{2}}, J_F, K^{\frac{1}{2}})$.

The normal stress component σ_{22} is continuous across the fault, while σ_{11} and σ_{33} are not. All three require partial derivative of v_2 along axis 3. The central difference is again substituted by the one-sided. Velocity $(v_2)_{I^{\frac{1}{2}},J_F,K}$ is acquired

from the condition on continuity of σ_{22} and v_2 across the fault. Equating right sides the elastodynamic equation (in the case of v_2) and Hooke's law (in the case of σ_{22}) on the $'+'$ and $'-'$ sides leads to (for spatialy constant λ and μ)

$$\frac{4(\lambda+2\mu)}{\Delta h}(v_2)_{I^{\frac{1}{2}},J_F,K} = \frac{2(\lambda+2\mu)}{\Delta h}\Big[(v_2)_{I^{\frac{1}{2}},J_F^{-\frac{1}{2}},K} + (v_2)_{I^{\frac{1}{2}},J_F^{\frac{1}{2}},K}\Big]$$
$$+\frac{\lambda}{\Delta h}\Big[-(D_1^{(2)}v_1^-)_{I^{\frac{1}{2}},J_F,K} - (D_3^{(2)}v_3^-)_{I^{\frac{1}{2}},J_F,K} + (D_1^{(2)}v_1^+)_{I^{\frac{1}{2}},J_F,K} + (D_3^{(2)}v_3^+)_{I^{\frac{1}{2}},J_F,K}\Big]. \tag{26}$$

One sided difference of v_2 is used to calculate the rest of the stress components at the fault:

$$\frac{(\sigma_{11}^{\pm})^{N^{\frac{1}{2}}}_{I^{\frac{1}{2}},J_F,K} - (\sigma_{11}^{\pm})^{N^{-\frac{1}{2}}}_{I^{\frac{1}{2}},J_F,K}}{\Delta t} = (\lambda+2\mu)(D_1^{(2)}v_1^{\pm})^N_{I^{\frac{1}{2}},J_F,K}$$
$$+\lambda(D_3^{(2)}v_3^{\pm})^N_{I^{\frac{1}{2}},J_F,K} \pm \lambda\frac{(v_2)^N_{I^{\frac{1}{2}},J_F,K} - (v_2)^N_{I^{\frac{1}{2}},J_F,K}}{\Delta h/2}, \tag{27}$$

$$\frac{(\sigma_{22})^{N^{\frac{1}{2}}}_{I^{\frac{1}{2}},J_F,K} - (\sigma_{22})^{N^{-\frac{1}{2}}}_{I^{\frac{1}{2}},J_F,K}}{\Delta t} = \lambda(D_1^{(2)}v_1^{\pm})^N_{I^{\frac{1}{2}},J_F,K}$$
$$+\lambda(D_3^{(2)}v_3^{\pm})^N_{I^{\frac{1}{2}},J_F,K} \pm (\lambda+2\mu)\frac{(v_2)^N_{I^{\frac{1}{2}},J_F,K} - (v_2)^N_{I^{\frac{1}{2}},J_F,K}}{\Delta h/2}, \tag{28}$$

$$\frac{(\sigma_{33}^{\pm})^{N^{\frac{1}{2}}}_{I^{\frac{1}{2}},J_F,K} - (\sigma_{33}^{\pm})^{N^{-\frac{1}{2}}}_{I^{\frac{1}{2}},J_F,K}}{\Delta t} = \lambda(D_1^{(2)}v_1^{\pm})^N_{I^{\frac{1}{2}},J_F,K}$$
$$+(\lambda+2\mu)(D_3^{(2)}v_3^{\pm})^N_{I^{\frac{1}{2}},J_F,K} \pm \lambda\frac{(v_2)^N_{I^{\frac{1}{2}},J_F,K} - (v_2)^N_{I^{\frac{1}{2}},J_F,K}}{\Delta h/2}. \tag{29}$$

The use of the second order FD causes unwanted high frequency oscillations. We follow Dalguer and Day (2007) and use an artificial viscous damping term of the forces $f_i^{\pm}$ to suppress them. The damped forces

$$\acute{f}_i^{\pm} = f_i^{\pm} + \eta\dot{f}_i^{\pm} \tag{30}$$

are used to calculate shear velocity components at the fault. The damping coefficient η depends on the time dicretisation $\eta = \eta_s\Delta t$, with an ideal value of η_s being 0.3. This value was determined experimentally by Dalguer and Day (2007) to have the lowest impact on rupture velocity speed. Dependence on Δt ties damping also to the space discretisation (via the CFL criterion) and damps amplitudes at frequencies close to the grid's Nyquist limit.

3 Linear slip-weakening friction

The linear slip-weakening friction law (Ida, 1972) is widely used in dynamic rupture simulations. The value of the effective friction coefficient depends only on the slip,

$$S = \sigma_n\mu_f(s). \tag{31}$$

For the rupture to propagate, the frictional force needs to decrease with continual sliding (slip-weakening). We consider linear slip-weakening relationship in the form introduced by Andrews (1976):

$$\mu_f(s) = \begin{cases} \mu_s - (\mu_s - \mu_d)s/D_c, & \text{if } s < D_c \\ \mu_d, & \text{if } s \geq D_c, \end{cases} \tag{32}$$

where μ_s, μ_d and D_c are initial model parameters: Static friction coefficient μ_s is a value of friction at the beginning of the sliding, friction then linearly drops to the dynamic friction $\mu_d < \mu_s$ over a characteristic slip-weakening distance D_c as shown in Fig. 3.

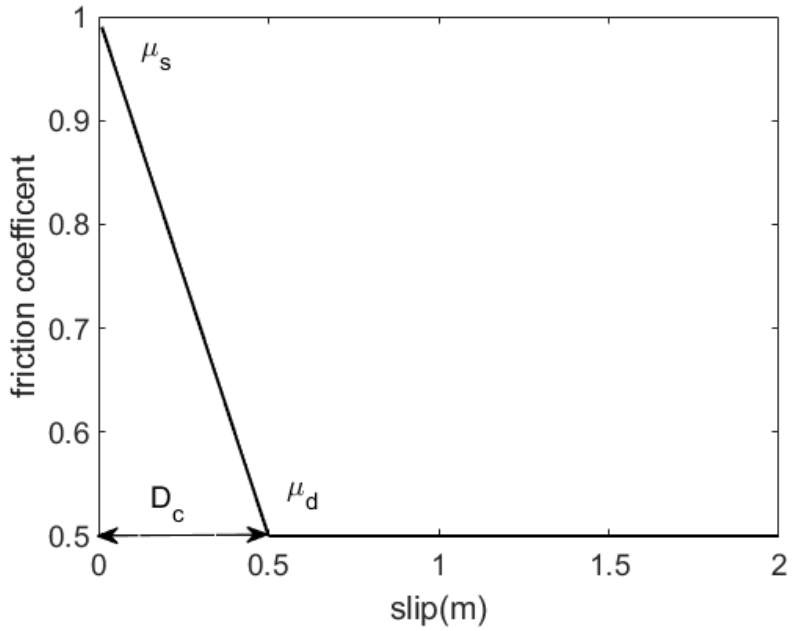

Figure 3: Linear slip-weakening friction law (bold line) with labeled values of static (μ_s) and dynamic (μ_d) friction coefficients. The characteristic slip distance D_c is marked by arrows.

The calculation of the frictional force during the dynamic rupture simulation requires knowledge of the slip at every time step. It is acquired by the integration of the slip rate $\dot{s}$. Using the time staggered position of the slip and slip rate, the integration is straightforward:

$$s^{N\frac{1}{2}} = s^{N^-\frac{1}{2}} + \Delta t \dot{s}^N. \tag{33}$$

The frictional strength can then be directly calculated as

$$S^{N\frac{1}{2}} = \begin{cases} \sigma_n[\mu_s - (\mu_s - \mu_d)s^{N\frac{1}{2}}/D_c], & \text{if } s^{N\frac{1}{2}} < D_c \\ \sigma_n \mu_d, & \text{if } s^{N\frac{1}{2}} \geq D_c. \end{cases} \tag{34}$$

4 Rate-and-state friction with fast-velocity-weakening

Rate-and-state type friction laws were developed by Dieterich (1986) and Ruina (1983) based on friction experiments with changing sliding velocity (velocity jump

and slide-hold-slide experiments). Friction depends on sliding velocity $\dot{s}$ and state variable ψ,

$$S = \sigma_n \mu_f(\dot{s}, \psi). \tag{35}$$

The state variable describes the state of the contacts at the surface boundary. It follows generally a slip-weakening law with contacts wearing down through sliding, i. e., ψ decreases during the sliding period. In addition to this behavior, increase of the state variable (and thus friction) during a period of slower sliding is possible, which simulates healing of the fracture. Behavior of the state is described by an evolution law, which is an ordinary differential equation:

$$\frac{d\psi}{dt} = F(s, \dot{s}, \psi). \tag{36}$$

Unlike the linear slip-weakening law, the rate-and-state type laws typically do not allow for the fault to stop sliding ($\dot{s} = 0$), we prescribe an initial non-zero slip rate $\dot{s}_{ini}$ acting as a numerical regularisation. The traction is set to be always equal to the frictional strength, meaning that only the second case in (5) applies.

Several versions of the fast-velocity-weakening law are employed in the literature (Dunham et al., 2011; Gabriel et al., 2012). We here implement the formulation used in SCEC/USGS benchmark suite (Harris et al., 2018). It consists of five interlinked equations:

$$\begin{aligned}
S &= \sigma_n a \ \mathrm{arcsinh}\Big[\frac{\dot{s}}{2\dot{s}_0}\exp\Big(\frac{\psi}{a}\Big)\Big], \\
\frac{d\psi}{dt} &= -\frac{\dot{s}}{L}[\psi - \psi_{SS}], \\
\psi_{SS} &= a \log\Big[\frac{2\dot{s}_0}{\dot{s}}\ \sinh\Big(\frac{f_{SS}}{a}\Big)\Big], \\
f_{SS} &= f_w + \frac{f_{LV} - f_w}{\Big[1 + (\dot{s}/\dot{s}_w)^8\Big]^{1/8}}, \\
f_{LV} &= f_0 - (b - a) \log\Big(\frac{\dot{s}}{\dot{s}_0}\Big).
\end{aligned} \tag{37}$$

Dynamic rupture simulations using rate-and-state friction are more complicated than in the linear slip-weakening case. The formulation requires the solution of two coupled differential equations at the fault boundary – one for the shear velocity components (slip rate) and the other for the state variable.

The following approach for the discretization and the solution of the velocity-state system of differential equations is extending the 2D approach presented in Rojas et al. (2009) to 3D. The specific procedure of solving the set of equations depends on the position of the velocity and state variable at discrete times. For the time staggered schemes, such as the scheme used in this work, the time-staggered distribution of slip rate and state variable (see Fig. 4) is a natural choice. The results are similarly accurate as if using a non-staggered distribution with high-order Rosenbrock integration (Rojas et al., 2009).

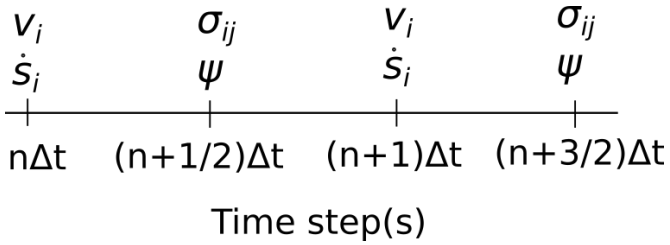

Figure 4: The time staggered position of slip rate and state variable

The first step is the integration of the evolution law for ψ (last four equations in (37)) in the interval between two succesive time steps $(N-1/2)\Delta t$ and $(N+1/2)\Delta t$. Due to the time-staggered distribution, velocity and slip rate are positioned in the middle of this interval $N\Delta t$, and are approximated by this value over the whole interval $\dot{s}(t) = (\dot{s})^N, \forall t \in \Big((N-1/2)\Delta t, (N+1/2)\Delta t\Big)$. With the slip rate constant over the whole interval, we integrate the differential equation in (37),

$$
\begin{aligned}
\psi^{N^{\frac{1}{2}}} &= (\psi^{N^{-\frac{1}{2}}} - \psi_{SS}(\dot{s}^N)) \exp(-\frac{\dot{s}^N \Delta t}{L}) + \psi_{SS}(\dot{s}^N), \\
\psi_{SS}(\dot{s}^N) &= a \log\Big[\frac{2s_0}{\dot{s}^N} \sinh\Big(\frac{f_{SS}(\dot{s}^N)}{a}\Big)\Big], \\
f_{SS}(\dot{s}^N) &= f_w + \frac{f_{LV}(\dot{s}^N) - f_w}{\Big[1 + (\dot{s}^N/s_w)^8\Big]^{1/8}}, \\
f_{LV}(\dot{s}^N) &= f_0 - (b-a) \log\Big(\frac{\dot{s}^N}{s_0}\Big).
\end{aligned}
\tag{38}
$$

The second step is the calculation of slip rate $(\dot{\mathbf{s}})^{N^1}$ from (25). First we calculate the updated absolute value of slip rate $\dot{s}^{N^1}$ in both nodes where slip rate components $\dot{s}_1$ and $\dot{s}_3$ are positioned, bilinear interpolation of $(R_i^-)^{N^{\frac{1}{2}}}$ in staggered nodes is also needed. The equation for $\dot{s}^{N^1}$ makes use of collinearity of traction and slip rate (18), leading to

$$
(\dot{s})^{N^1} = -\frac{4\Delta t}{\Delta h \rho}(T)^{N^{\frac{1}{2}}} + \left|(\dot{\mathbf{s}})^N - \frac{4\Delta t}{\Delta h \rho}\left[(\mathbf{R}^-)^{N^{\frac{1}{2}}} - \mathbf{T}_1^0\right]\right|. \tag{39}
$$

Since the fault is assumed to be always sliding, the absolute value of shear traction $(T)^{N^{\frac{1}{2}}}$ is equal to friction S from the first equation of (37):

$$
(\dot{s})^{N^1} = -\frac{4\Delta t}{\Delta h \rho} S(\dot{s}^?, \psi^{N^{\frac{1}{2}}}) + \left|(\dot{\mathbf{s}})^N - \frac{4\Delta t}{\Delta h \rho}\left[(\mathbf{R}^-)^{N^{\frac{1}{2}}} - \mathbf{T}_1^0\right]\right|. \tag{40}
$$

The slip rate $\dot{s}^?$ on the right hand side of (40) cannot be set to the value of slip rate in the previous time step $\dot{s}^? = (\dot{s})^N$ (Forward Euler method), because the resulting scheme is highly unstable. Especially for small values of the slip rate the derivative of $\operatorname{arcsinh}(x)$ has its highest value. A backward Euler scheme ($\dot{s}^? = \dot{s}^{N^1}$) or trapezoidal scheme ($\dot{s}^? = (\dot{s}^N + \dot{s}^{N^1})/2$) need to be used instead. Although the trapezoidal scheme offers higher order accuracy, accuracy improvement in our practical applications are minimal.

The Backward Euler scheme is used in FD3D_TSN, yielding

$$(\dot{s})^{N^1} = (\tilde{\dot{s}})^N + C \ \mathrm{arcsinh}\Big[\frac{(\dot{s})^{N^1}}{2s_0}\exp\Big(\frac{\psi^{N^{\frac{1}{2}}}}{a}\Big)\Big], \tag{41}$$

where

$$(\tilde{\dot{s}})^N = \left|(\dot{\mathbf{s}})^N - \frac{4\Delta t}{\Delta h \rho}\left[(\mathbf{R}^-)^{N^{\frac{1}{2}}} - \mathbf{T}_1^0\right]\right| \tag{42}$$

denotes the part of the equation (39) already explicitly calculated before the time step $(n+1)\Delta t$, and

$$C = \frac{4\Delta t}{\Delta h \rho}\sigma_n a. \tag{43}$$

Equation (41) is nonlinear and needs to be solved accordingly, for example by the Newton's method, whose application we describe below.

We want to find a new slip rate value $(\dot{s})^{N^1}$ that satisfies equation (41). This is equivalent to finding a root of function

$$F\left((\dot{s})^{N^1}\right) = (\tilde{\dot{s}})^N - (\dot{s})^{N^1} + C \ \mathrm{arcsinh}\Big[\frac{(\dot{s})^{N^1}}{2s_0}\exp\Big(\frac{\psi^{N^{\frac{1}{2}}}}{a}\Big)\Big]. \tag{44}$$

We modify it to simplify finding the solution by substitution of a variable

$$w = \ \mathrm{arcsinh}\Big[\frac{(\dot{s})^{N^1}}{2s_0}\exp\Big(\frac{\psi^{N^{\frac{1}{2}}}}{a}\Big)\Big]. \tag{45}$$

This leads to a simple form of the function:

$$F(w) = (\tilde{\dot{s}})^N + Cw - \exp\Big(\frac{-\psi^{N^{\frac{1}{2}}}}{a}\Big)2s_0\mathrm{sinh}(w), \tag{46}$$

In Newton's method the root w of the function $F(x)$, is found approximately by a succesive iteration:

$$w_{n+1} = w_n - \frac{F(w_n)}{F'(w_n)}, \tag{47}$$

where F' is the derivative of function F, and w_n is the approximate value of the root at the n-th iteration.

The derivative of (46) is

$$F'(w) = C - \exp\Big(\frac{-\psi^{N^{\frac{1}{2}}}}{a}\Big)2s_0\mathrm{cosh}(w). \tag{48}$$

The natural choice of the starting value of w is its value at the previous time step:

$$w_0 = \ \mathrm{arcsinh}\Big[\frac{(\dot{s})^{N}}{2s_0}\exp\Big(\frac{\psi^{N^{\frac{1}{2}}}}{a}\Big)\Big]. \tag{49}$$

Equation (47) is then applied iteratively until the difference between successive values of w (the error of the approximation) is lower than a chosen value – in our

implementation 10^{-5} and 10^{-10} for single and double precision, respectively. The value of slip rate solving (41) is calculated from the substitution (45):

$$(\dot{s})^{N^1} = 2s_0 \sinh(w)\exp\Big(-\frac{\psi^{N^{\frac{1}{2}}}}{a}\Big). \tag{50}$$

Components of the updated slip rate are found from collinearity of the slip rate and the traction (6):

$$(\dot{\mathbf{s}})^{N^1} = (\dot{s})^{N^1}\frac{(\mathbf{T})^{N^{\frac{1}{2}}}}{(T)^{N^{\frac{1}{2}}}}. \tag{51}$$

The discrete solution of the fault boundary conditions with the fast-velocity-weakening rate-and-state law using the traction-at-split-node method consists of the application of equations (38) to update the value of the state variable and Newton's method solution of (41) to update the slip rate. This is done at every node at the fault surface independently.

Bibliography

Andrews, D. J. (1976). Rupture velocity of plane strain shear cracks. *J. Geophys. Res.*, 81(32):5679– 5687.

Cruz-Atienza, V. M., Virieux, J., and Aochi, H. (2007). 3d finite-difference dynamic-rupture modeling along nonplanar faults. *Geophysics*, 72(5):SM123–SM137.

Dalguer, L. A. and Day, S. M. (2007). Staggered-grid split-node method for spontaneous rupture simulation. *J. Geophys. Res. Solid Earth*, 112, B02302.

Dieterich, J. H. (1986). A model for the nucleation of earthquake slip. *Washington DC American Geophysical Union Geophysical Monograph Series*, 37.

Dunham, E. M., Belanger, D., Cong, L., and Kozdon, J. E. (2011). Earthquake ruptures with strongly rate-weakening friction and off-fault plasticity, part 1: Planar faults. *Bull. Seis. Soc. Am.*, 101:2296–2307.

Duru, K. and Dunham, E. M. (2016). Dynamic earthquake rupture simulations on nonplanar faults embedded in 3d geometrically complex, heterogeneous elastic solids. *J. Comput. Phys.*, 305:185 – 207.

Duru, K., Rannabauer, L., Gabriel, A.-A., and Igel, H. (2018). A new discontinuous galerkin spectral element method for elastic waves with physically motivated numerical fluxes.

Gabriel, A., Ampuero, J., Dalguer, L. A., and Mai, P. M. (2012). The transition of dynamic rupture styles in elastic media under velocity-weakening friction. *J. Geophys. Res.*, 117, B09311.

Harris, R. A., Barall, M., Aagaard, B., Ma, S., Roten, D., Olsen, K., Duan, B., Liu, D., Luo, B., Bai, K., Ampuero, J., Kaneko, Y., Gabriel, A., Duru, K., Ulrich, T., Wollherr, S., Shi, Z., Dunham, E., Bydlon, S., Zhang, Z., Chen, X., Somala, S. N., Pelties, C., Tago, J., Cruz-Atienza, V. M., Kozdon, J., Daub, E., Aslam, K., Kase, Y., K.Withers, and Dalguer, L. (2018). A suite of exercises for verifying dynamic earthquake rupture codes. *Seismol. Res. Lett.*, 89(3):1146–1162.

Ida, Y. (1972). Cohesive force across the tip of a longitudinal-shear crack and griffith's specific surface energy. *J. Geophys. Res.*, 77(20):3796–3805.

Rojas, O., Dunham, E. M., Day, S. M., Dalguer, L. A., and Castillo, J. E. (2009). Finite difference modelling of rupture propagation with strong velocity-weakening friction. *Geophys. J. Int.*, 179(3):1831–1858.

Ruina, A. (1983). Slip instability and state variable friction laws. *J. Geophys. Res.*, 88(B12):10359– 10370.